

Article

Fractional Power-Law Intraband Optical Conductivity in the Low-Dimensional Dirac Material CaMnBi_2

M. B. Schilling¹, C. X. Wang², Y. G. Shi², R. K. Kremer³ , M. Dressel¹  and A. V. Pronin^{1,*}

¹ Physikalisches Institut, Universität Stuttgart, 70569 Stuttgart, Germany; micha.physiker@gmx.de (M.B.S.); martin.dressel@pi1.physik.uni-stuttgart.de (M.D.)

² Beijing National Laboratory for Condensed Matter Physics, Institute of Physics, Chinese Academy of Sciences, Beijing 100190, China; cxwang@iphy.ac.cn (C.X.W.); ygshi@iphy.ac.cn (Y.G.S.)

³ Max-Planck-Institut für Festkörperforschung, 70569 Stuttgart, Germany; rekre@fkf.mpg.de

* Correspondence: artem.pronin@pi1.physik.uni-stuttgart.de

Abstract: We studied the broadband optical conductivity of CaMnBi_2 , a material with two-dimensional Dirac electronic bands, and found that both components of the intraband conductivity follow a universal power law as a function of frequency at low temperatures. This conductivity scaling differs from the Drude(-like) behavior, generally expected for free carriers, but matches the predictions for the intraband response of an electronic system in a quantum critical region. Since no other indications of quantum criticality are reported for CaMnBi_2 so far, the cause of the observed unusual scaling remains an open question.

Keywords: Dirac materials; optical-conductivity scaling; topological semimetals



Citation: Schilling, M.B.; Wang, C.X.; Shi, Y.G.; Kremer, R.K.; Dressel, M.; Pronin, A.V. Fractional Power-Law Intraband Optical Conductivity in the Low-Dimensional Dirac Material CaMnBi_2 . *Crystals* **2021**, *11*, 428. <https://doi.org/10.3390/cryst11040428>

Academic Editor: Andreas Hermann

Received: 30 March 2021

Accepted: 13 April 2021

Published: 16 April 2021

Publisher's Note: MDPI stays neutral with regard to jurisdictional claims in published maps and institutional affiliations.



Copyright: © 2021 by the authors. Licensee MDPI, Basel, Switzerland. This article is an open access article distributed under the terms and conditions of the Creative Commons Attribution (CC BY) license (<https://creativecommons.org/licenses/by/4.0/>).

1. Introduction

CaMnBi_2 and its sister compound SrMnBi_2 are some of the first materials in which bulk electronic bands with Dirac-like dispersion were experimentally confirmed [1,2]. Both materials are arranged in layers with square nets of Bi atoms (space group $P4/nmm$). The materials are believed to possess two-dimensional Dirac bands that are anisotropic and slightly gapped due to spin-orbit coupling [1–5]. The materials have antiferromagnetic in-plane ordering of Mn ions with Néel temperatures between 270 and 290 K [1,3,6,7]. In CaMnBi_2 , another transition at $T_s \approx 50$ K was detected by various experimental techniques including transport [2,3,8,9], magnetoresistance [2], susceptibility [3], thermopower [8], and optical [10,11] measurements. The signatures of T_s are often tiny and not always resolved in DC transport [6]. No indications of a phase transition were detected in specific-heat [3] and neutron measurements [7]. The anomaly at T_s was first tentatively attributed to either weak ferromagnetic order [2] or spin canting [3]. Based on optical and magnetic torque measurements in combination with band-structure calculations, Yang et al. [11] recently concluded on a spin-canting-induced band reconstruction at T_s , therefore clarifying the nature of this transition. In this paper, we report on the optical conductivity measurements in CaMnBi_2 . Below T_s , we found an unusual scaling of its intraband conductivity. This scaling was previously attributed to manifestations of quantum criticality. Hence, it might be an indication of quantum criticality in CaMnBi_2 , although other explanations cannot be excluded.

2. Materials and Methods

Sample growth and characterization: single crystals of CaMnBi_2 were grown using a self-flux method similar to that described previously [6]. Elementary Ca (99.99%), Mn (99.9%), and Bi (99.99%) were mixed in the molar ratio Ca:Mn:Bi = 1:1:8 and put into an alumina tube before sealing it in a quartz tube. The mixture was heated up to 800 °C during 10 h, kept at this temperature for 5 h, then slowly cooled down to 450 °C at a

rate of 3 °C/h. The excess Bi flux was decanted at this temperature in a centrifuge. As CaMnBi_2 is somewhat air-sensitive, its handling was carried out in an inert gas atmosphere. The obtained samples were carefully characterized by X-ray, transport, magnetic, and specific-heat measurements as described in the Appendix A.

Optical measurements: the near-normal-incidence optical reflectivity $R(\nu)$ was measured from a large (roughly 2 by 3 mm) (001) surface of a CaMnBi_2 crystal at a number of temperatures between 10 to 300 K over a broad frequency range from $\nu = 50$ to $22,000 \text{ cm}^{-1}$ ($\approx 6 \text{ meV}$ – 2.75 eV) using two Fourier-transform spectrometers (Bruker IFS 113v and Bruker Vertex 80v equipped with a Hyperion IR microscope (all three devices are from Bruker Corporation, Billerica, MA, USA)). At low frequencies, an in situ gold evaporation technique was utilized for reference measurements. For frequencies above 1000 cm^{-1} , gold and protected silver mirrors served as references. The complex optical conductivity, $\sigma(\nu) = \sigma_1(\nu) + i\sigma_2(\nu)$, was obtained using Kramers–Kronig transformations. The high-frequency range was extended by involving the X-ray atomic scattering functions for high-frequency extrapolations [12]. The results of the four-point DC resistivity measurements were used for the low-frequency extrapolations. To avoid possible surface oxidation, all measurements were performed on freshly cleaved surfaces.

3. Results

The results of our optical experiments are shown in Figures 1 and 2. All measurements were obtained on (001) planes of CaMnBi_2 (in-plane response). Let us note here that, although the in-plane Dirac bands of CaMnBi_2 are known to be highly anisotropic [4,5], this band anisotropy is not expected to be seen in the linear optical response because of the four-fold in-plane symmetry. Indeed, our polarization-dependent reflectivity measurements do not reveal any optical anisotropy. Hence, we discuss the measurements performed with unpolarized light throughout the paper.

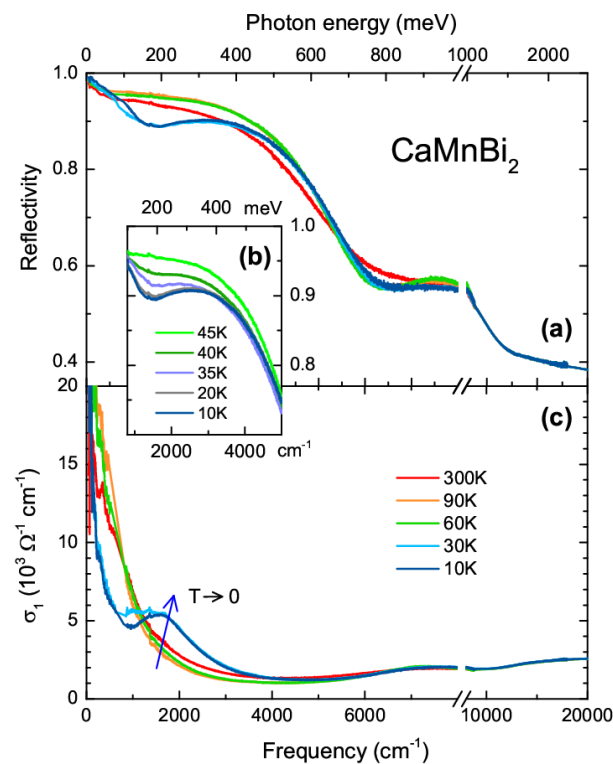


Figure 1. Frequency-dependent in-plane reflectivity $R(\nu)$ (panels (a,b)) and the real part of the optical conductivity $\sigma_1(\nu)$ (panel (c)) of CaMnBi_2 for select temperatures between 10 and 300 K. The development of a dip in $R(\nu)$ and a bump in $\sigma_1(\nu)$ at around 1500 cm^{-1} ($\approx 200 \text{ meV}$) is clearly seen at $T < 50 \text{ K}$ and marked with the arrow in panel (c). Note the change in frequency scale at 8000 cm^{-1} .

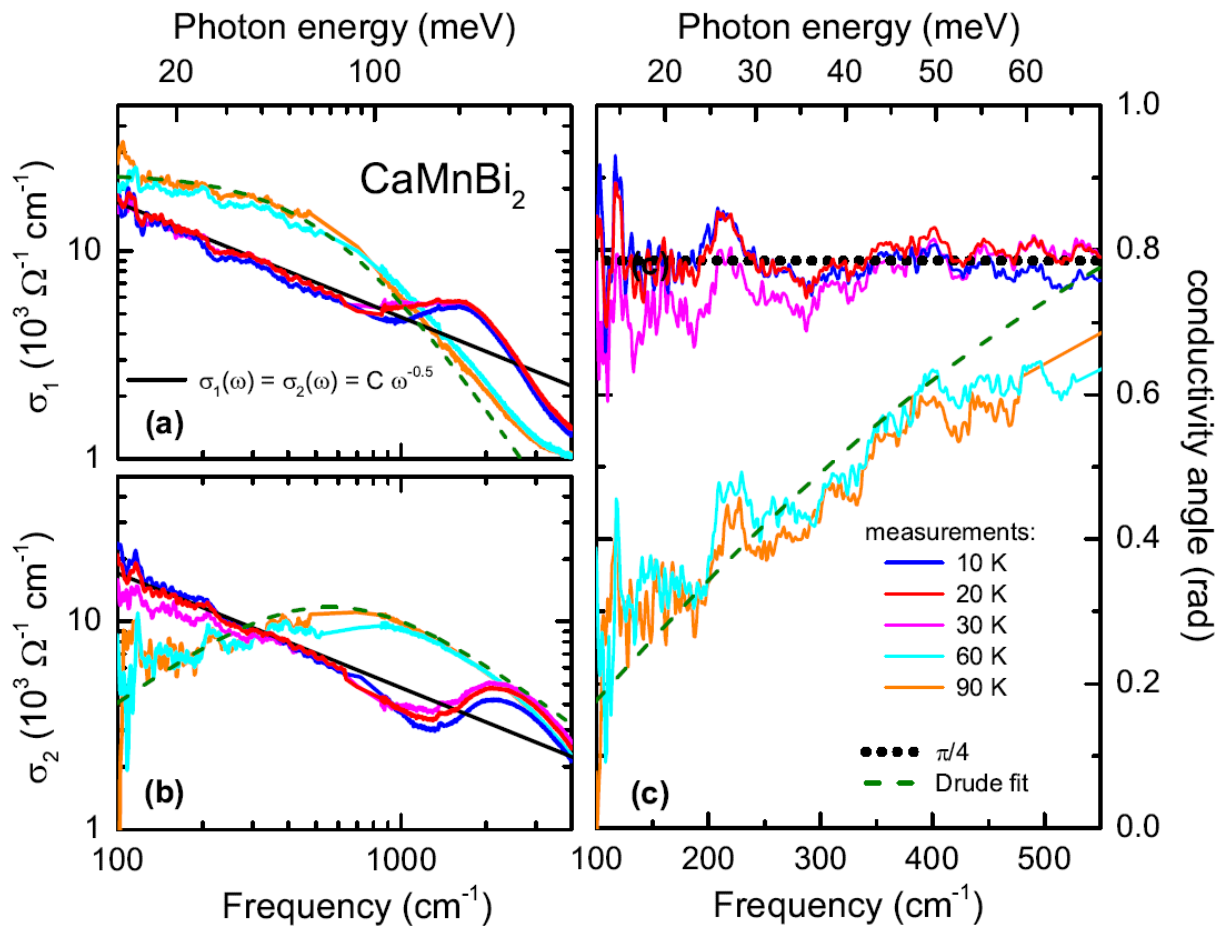


Figure 2. Scaling of the intraband complex optical conductivity in CaMnBi₂. The real (panel (a)) and imaginary (panel (b)) parts of the optical conductivity follow the Drude behavior for $T > T_s \sim 50$ K and scale as $1/\omega^{0.5}$ at low temperatures. The conductivity angle φ (panel (c)) is almost constant at these temperatures, while it increases quasi-linearly in the Drude case.

The obtained broadband optical spectra as functions of frequency are shown in Figure 1. The interband part of the optical conductivity has been analyzed in Reference [11]; our experimental findings are in full agreement with these results. The goal of our paper is to analyze the intraband low-energy response.

At low frequencies and for $T > 50$ K, the reflectivity $R(\nu)$ [$\nu = \omega/(2\pi)$] and both parts of the complex conductivity are dominated by intraband electronic transitions and are typically metallic: $R(\nu)$ approaches unity as ν diminishes, while $\sigma_1(\nu)$ and $\sigma_2(\nu)$ reveal typical Drude behavior, as can be seen best from Figure 2a,b. The conductivity angle, $\varphi = \arctan(\sigma_2/\sigma_1)$, is frequency dependent and follows the Drude model; see panel (c).

The low-energy interband transitions within the Dirac bands, which are known to provide a power-law contribution to low-frequency $\sigma_1(\nu)$ [13–17], are not seen in our measurements. The low-frequency response of CaMnBi₂ is completely dominated by free carriers. This situation is, in fact, rather typical for different Dirac systems, in which the Fermi level is situated far from the band crossings and/or the free-carrier contributions from non-Dirac bands are significant [18–23].

At the spin-canting temperature $T_s \approx 50$ K, dramatic changes occur in the optical spectra. Apart from the formation of a low-frequency mode at approximately 200 meV (Figure 2a,b) and a corresponding dip in reflectivity (Figure 1a) that were reported previously [10,11], the intraband absorption also drastically changes its shape. The single Drude term is unable to describe the low-energy spectra. (Let us note that the two-Drude approach used in Reference [11] is able to provide only a very rough description of the experimental $\sigma_1(\omega)$; see Figure 1b of Reference [11].) Instead, one can see that both components of the

optical conductivity follow a power law. This power-law behavior is most apparent at low temperatures: below 30 K. As evidenced from our fit, $\sigma_1(\omega)$ and $\sigma_2(\omega)$ both depend on frequency as $1/\omega^{0.5}$; this power law is shown as black solid lines in Figure 2a,b. This behavior of conductivity strongly differs from the conventional Drude response. In particular, changes in the reactive part ($\sigma_2(\omega)$) are significant: instead of showing a broad maximum (which corresponds to the scattering rate in the Drude case), $\sigma_2(\omega)$ is now monotonic in frequency. Furthermore, the pre-factors in the frequency dependencies of $\sigma_1(\omega)$ and $\sigma_2(\omega)$ are identical, i.e., σ_1 and σ_2 are equal at a given frequency. This provides that $\varphi = \pi/4$.

4. Discussion

The strong non-Drude intraband response of CaMnBi₂ is rather surprising. Free electrons are generally expected to follow a Drude(-like) conductivity ansatz [24]. One can notice that the conductivity scaling observed here was widely discussed in the past in relation to quantum phase transitions (QPTs). The presence of a QPT leads to universal power-law scaling behaviors of the response functions [25]. In particular, the frequency-dependent complex conductivity should follow such a behavior. For the frequency region where $k_B T < \hbar\omega$, the conductivity can be a universal function of frequency [25]. In our case, this inequality is fulfilled. Van der Marel et al. [26] argued that scale invariance, causality, and time reversal symmetry require that, for a quantum critical system, the complex conductivity in this frequency region follows:

$$\sigma(\omega) = |\sigma(\omega)|e^{i\varphi(\omega)} = C\omega^{\gamma-2}e^{i\pi(1-\gamma/2)}, \quad (1)$$

where γ is a critical exponent and C is a constant. This ansatz implies that both $\sigma_1(\omega)$ and $\sigma_2(\omega)$ depend on frequency as $\omega^{\gamma-2}$ and the phase φ is frequency independent and set by the same exponent γ . If we apply Equation (1) to the recorded spectra of σ_1 and σ_2 , we find the critical exponent γ to be 3/2. According to the scaling analysis, this value of the critical exponent should provide a frequency-independent value for the conductivity angle, $\varphi = \pi/4$. As noticed above, this result indeed follows from our data.

Interestingly, the same optical conductivity scaling (with $\gamma = 3/2$) was theoretically elaborated by Ioffe and Millis [27] in relation to a possible QPT in the superconducting cuprates. Van der Marel [28] suggested a generalized form of this relation (with the critical exponent not fixed at 3/2) that merges with a proposition of Anderson [29] for a one-dimensional Luttinger liquid in the collision-less limit.

It should be noted that the Dirac bands in CaMnBi₂ are two-dimensional (due to the planar net of Bi atoms) and that they possess a very high anisotropy within this plane [4,5]. In fact, the electronic band structure can be viewed as a gapped dispersive nodal line in two dimensions, with the Fermi velocity in one direction being much smaller than the Fermi velocity in another one. It is known that the presence of a nodal line effectively reduces the dimensionality of electronic transport [16,17,30]. This reduction can possibly occur in CaMnBi₂, leading to a quasi-one-dimensional situation and, eventually, to the realization of a quantum critical state.

Certainly, the nature of the observed scaling has to be clarified in further theoretical and experimental studies; the observed scaling is not necessarily related to quantum criticality. The goal of this paper is to report this unusual conductivity behavior and to suggest a possible explanation. Still, one can note that the possible quantum criticality in CaMnBi₂ (if it is confirmed) should likely be related to the magnetism in this system and, particularly, to the spin-canting transition at T_s . This conclusion follows from the fact that the observed conductivity scaling appears only below this temperature.

5. Conclusions

In summary, we performed broadband optical conductivity measurements of CaMnBi₂—a highly anisotropic material with two-dimensional nets of Bi atoms and anisotropic Dirac bands. We detected the formation of a finite-frequency absorption mode at $T < T_s = 50$ K, which is in agreement with previous studies. Most importantly, the optical response of

itinerant electrons at these temperatures is not of the Drude type. Instead, it follows a fractional power-law behavior, $\sigma_1(\omega) \sim \sigma_2(\omega) \sim \omega^{-0.5}$, that is similar to the behavior proposed for quantum critical systems with the critical exponent $\gamma = 3/2$. These findings might indicate that CaMnBi_2 is in the vicinity of a quantum phase transition. More input from the theory side and further experiments are necessary to confirm this proposition.

Author Contributions: Conceptualization, A.V.P.; sample growth, C.X.W. and Y.G.S.; measurements, M.B.S. and R.K.K.; data analysis, M.B.S. and A.V.P.; writing—original draft preparation, M.B.S.; writing—review and editing, M.D. and A.V.P.; funding acquisition, Y.G.S., M.D. and A.V.P. All authors have read and agreed to the published version of the manuscript.

Funding: This work was partly funded by the Deutsche Forschungsgemeinschaft (DFG) via grant No. DR228/51-3 and by K. C. Wong Education Foundation (GJTD-2018-01).

Institutional Review Board Statement: Not applicable.

Informed Consent Statement: Not applicable.

Data Availability Statement: The data sets generated and analyzed during the current study are available from the corresponding author upon request.

Acknowledgments: We thank Vladimir Juričić and Run Yang for useful discussions and Gabriele Untereiner for technical support.

Conflicts of Interest: The authors declare no conflict of interest. The funders had no role in the design of the study; in the collection, analyses, or interpretation of data; in the writing of the manuscript; or in the decision to publish the results.

Appendix A

Electronic transport and magnetic susceptibility: temperature-dependent DC resistivity, $\rho(T)$, was measured in a custom-made setup at temperatures down to 2 K. To highlight the discussed feature in resistivity near T_s , we plot $\rho(T)$ on an enlarged scale in Figure A1a. To further confirm the T_s feature, we performed temperature-dependent measurements of magnetic susceptibility, $\chi(T)$, at 2 T down to 10 K with a commercial setup (MPMS, Quantum Design Inc., San Diego, CA, USA) based on a superconducting quantum interference device. The results of these measurements are shown in Figure A1b. To clearly observe the anomaly at T_s , we performed a polynomial fit of the $\chi(T)$ curve at $T > T_s$ and subtracted the fit from the experimental data. The value of $\Delta\chi(T)$ obtained in this way is shown in Figure A1c. For $T \ll T_s$, $\Delta\chi(T)$ remains almost constant.

Heat-capacity measurements: heat capacity was measured as a function of temperature, employing the relaxation method (PPMS, Quantum Design Inc., San Diego, CA, USA). The sample was attached with Apiezon N vacuum grease to the sapphire platform, and the heat capacity of this platform (including the vacuum grease) was measured in advance and then subtracted from the total heat capacity. Figure A1d displays our results of the specific-heat measurements. The data reveal a small λ -type anomaly at 290 K, which is associated with the antiferromagnetic ordering of Mn atoms. The Néel temperature is in good agreement with that reported by Guo et al. [6] from neutron powder diffraction data and is slightly higher than the findings in other reports [3,7]. The low-temperature C_p/T data can be well fitted with a power law, $C_p/T = \gamma + \beta T^2 + \delta T^4 + \varepsilon T^6$, with the Sommerfeld term $\gamma = 6.78 \text{ mJ}/(\text{molK}^2)$. The higher powers of this polynomial represent the lattice and magnon contributions. They are very small and amount to $\beta = 0.00126(1) \text{ J}/(\text{molK}^4)$, $\delta = 2.04(3) \times 10^{-5} \text{ J}/(\text{molK}^6)$, and $\varepsilon = -9.3(2) \times 10^{-8} \text{ J}/(\text{molK}^8)$. Most importantly, C_p/T is featureless at T_s and in agreement with a previous report [3].

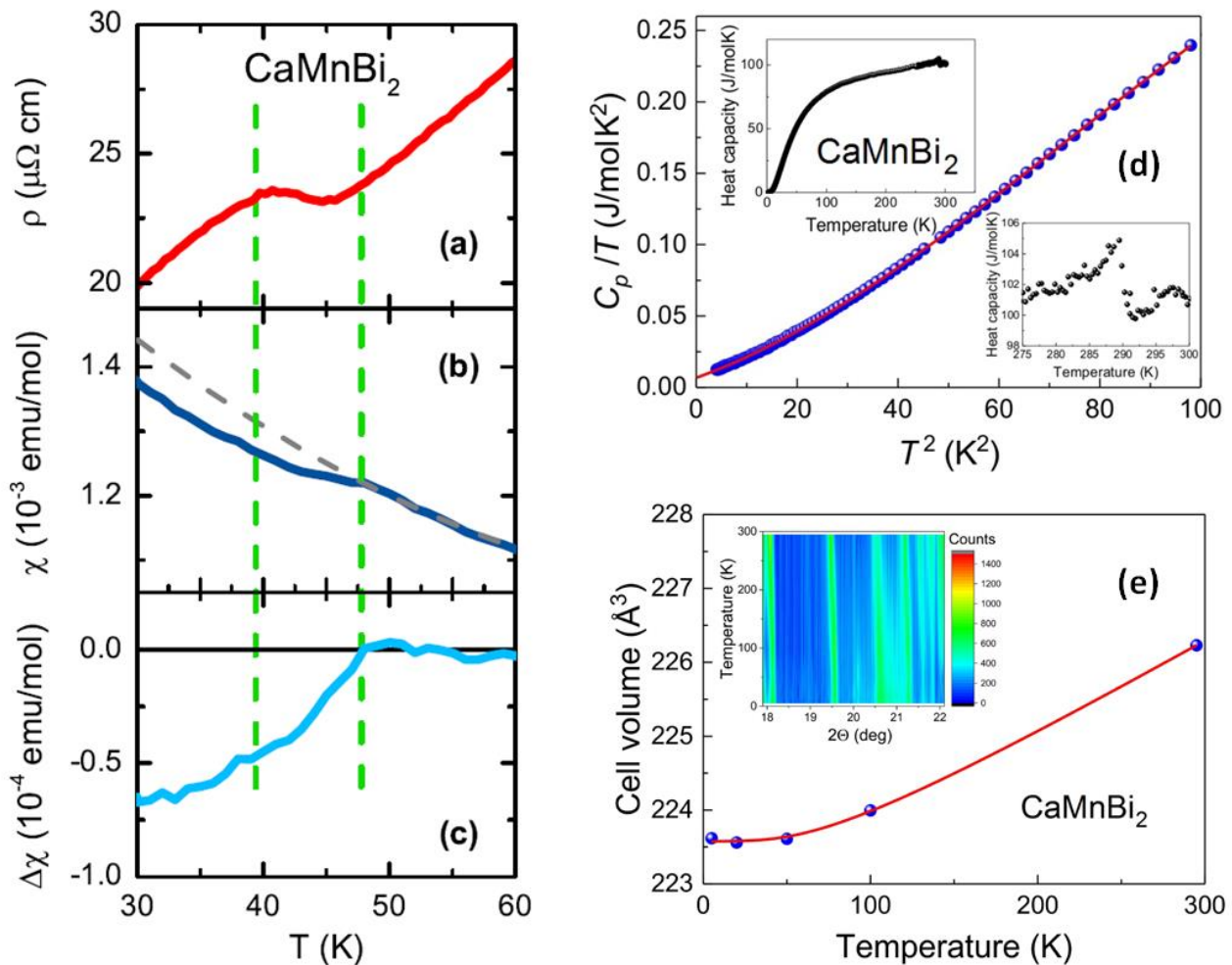


Figure A1. Characterization measurements of CaMnBi_2 . DC resistivity $\rho(T)$ (a), magnetic susceptibility $\chi(T)$ (b), and the deviation of $\chi(T)$ from its high-temperature behavior (c). The data in panels (a–c) are shown at the temperatures near T_s to highlight the presence of a transition. Molar specific heat (d). The main frame shows a Sommerfeld plot (blue circles) with a fit (red line) to a polynomial in T^2 (see text). The insets provide an overview on a linear temperature scale and a magnification around the 290 K anomaly. The unit cell volume is shown as a function of temperature in panel (e). The red solid line represents a fit of the experimental data to Equation (A1) with the parameters given in the text. The inset displays a section of the diffraction pattern ($\lambda = 0.709319 \text{ \AA}$) versus Bragg angle 2Θ and temperature. The Bragg reflections shown are indexed as 200 at 18.15° , 114 at 19.58° , 105 at 20.60° , 211 at 20.65° , 203 at 21.30° , and 212 at 21.63° .

X-ray measurements: in order to check the structural aspect, we performed temperature-dependent X-ray powder diffraction measurements at 295, 100, 50, 20, and 5 K. The X-ray patterns were collected on a CaMnBi_2 sample contained in a 0.3-mm diameter quartz glass capillary under He exchange gas using $\text{Mo K}\alpha_1$ radiation. Temperatures between 295 and 5 K were adjusted in a home-built cryostat. As revealed in Figure A1e, there are no visible splittings or broadenings of the Bragg reflections, which would be indicative of a structural phase transition. The tetragonal lattice parameters were obtained from Rietveld profile refinements of the diffraction patterns assuming the space group $P4/nmm$ (No. 129) and the atom and lattice parameters reported by Brechtel et al. [31] as starting parameters. They perfectly follow a simple Debye law:

$$V(T) = V_0 + I_v T \frac{T}{\Theta_D^3} \int_0^{\Theta_D/T} \frac{x^3}{e^x - 1} dx, \quad (\text{A1})$$

with $V_0 = 223.58(3) \text{ \AA}^3$, $\Theta_D = 279(4) \text{ K}$, and $I_V = 0.0130(7) \text{ \AA}^3$ (here, V_0 is the unit-cell volume at 0 K, Θ_D is the Debye temperature, and the pre-factor I_V is a linear function of the Grüneisen parameter in the Debye approximation [32]). As seen from Figure A1e, no anomalies in the thermal expansion, which could indicate a structural phase transition, were detected. This is consistent with the absence of broadenings or splittings of the Bragg reflections. Thus, any detectable structural transition at T_s is excluded.

References

- Park, J.; Lee, G.; Wolff-Fabris, F.; Koh, Y.Y.; Eom, M.J.; Kim, Y.K.; Farhan, M.A.; Jo, Y.J.; Kim, C.; Shim, J.H.; et al. Anisotropic Dirac Fermions in a Bi Square Net of SrMnBi₂. *Phys. Rev. Lett.* **2011**, *107*, 126402. [[CrossRef](#)] [[PubMed](#)]
- Wang, K.; Graf, D.; Wang, L.; Lei, H.; Tozer, S.W.; Petrovic, C. Two-dimensional Dirac fermions and quantum magnetoresistance in CaMnBi₂. *Phys. Rev. B* **2012**, *85*, 041101(R). [[CrossRef](#)]
- He, J.B.; Wang, D.M.; Chen, G.F. Giant magnetoresistance in layered manganese pnictide CaMnBi₂. *Appl. Phys. Lett.* **2012**, *100*, 112405. [[CrossRef](#)]
- Lee, G.; Farhan, M.A.; Kim, J.S.; Shim, J.H. Anisotropic Dirac electronic structures of AMnBi₂ (A = Sr, Ca). *Phys. Rev. B* **2013**, *87*, 245104. [[CrossRef](#)]
- Feng, Y.; Wang, Z.; Chen, C.; Shi, Y.; Xie, Z.; Yi, H.; Liang, A.; He, S.; He, J.; Peng, Y.; et al. Strong Anisotropy of Dirac Cones in SrMnBi₂ and CaMnBi₂ Revealed by Angle-Resolved Photoemission Spectroscopy. *Sci. Rep.* **2014**, *4*, 5385. [[CrossRef](#)] [[PubMed](#)]
- Guo, Y.F.; Princep, A.J.; Zhang, X.; Manuel, P.; Khalyavin, D.; Mazin, I.I.; Shi, Y.G.; Boothroyd, A.T. Coupling of magnetic order to planar Bi electrons in the anisotropic Dirac metals AMnBi₂ (A = Sr, Ca). *Phys. Rev. B* **2014**, *90*, 075120. [[CrossRef](#)]
- Rahn, M.C.; Princep, A.J.; Piovano, A.; Kulda, J.; Guo, Y.F.; Shi, Y.G.; Boothroyd, A.T. Spin dynamics in the antiferromagnetic phases of the Dirac metals AMnBi₂ (A = Sr, Ca). *Phys. Rev. B* **2017**, *95*, 134405. [[CrossRef](#)]
- Wang, K.; Wang, L.; Petrovic, C. Large magnetothermopower effect in Dirac materials (Sr/Ca)MnBi₂. *Appl. Phys. Lett.* **2012**, *100*, 112111.
- Wang, A.; Graf, D.; Wu, L.; Wang, K.; Bozin, E.; Zhu, Y.; Petrovic, C. Interlayer electronic transport in CaMnBi₂ antiferromagnet. *Phys. Rev. B* **2016**, *94*, 125118. [[CrossRef](#)]
- Corasaniti, M.; Yang, R.; Pal, A.; Chinotti, M.; Degiorgi, L.; Wang, A.; Petrovic, C. Fermi surface gapping in the Dirac material Ca_{1-x}Na_xMnBi₂. *Phys. Rev. B* **2019**, *100*, 041107. [[CrossRef](#)]
- Yang, R.; Corasaniti, M.; Le, C.C.; Liao, Z.Y.; Wang, A.F.; Du, Q.; Petrovic, C.; Qiu, X.G.; Hu, J.P.; Degiorgi, L. Spin-Canting-Induced Band Reconstruction in the Dirac Material Ca_{1-x}Na_xMnBi₂. *Phys. Rev. Lett.* **2020**, *124*, 137201. [[CrossRef](#)]
- Tanner, D.B. Use of x-ray scattering functions in Kramers-Kronig analysis of reflectance. *Phys. Rev. B* **2015**, *91*, 035123. [[CrossRef](#)]
- Hosur, P.; Parameswaran, S.A.; Vishwanath, A. Charge Transport in Weyl Semimetals. *Phys. Rev. Lett.* **2012**, *108*, 046602. [[CrossRef](#)] [[PubMed](#)]
- Bácsi, Á.; Virosztek, A. Low-frequency optical conductivity in graphene and in other scale-invariant two-band systems. *Phys. Rev. B* **2013**, *87*, 125425. [[CrossRef](#)]
- Ashby, P.E.C.; Carbotte, J.P. Chiral anomaly and optical absorption in Weyl semimetals. *Phys. Rev. B* **2014**, *89*, 245121. [[CrossRef](#)]
- Ahn, S.; Mele, E.J.; Min, H. Electrodynamics on Fermi Cyclides in Nodal Line Semimetals. *Phys. Rev. Lett.* **2017**, *119*, 147402. [[CrossRef](#)]
- Carbotte, J.P. Optical response of a line node semimetal. *J. Phys. Condens. Matter* **2017**, *29*, 045301. [[CrossRef](#)]
- Schilling, M.B.; Löhle, A.; Neubauer, D.; Shekhar, C.; Felser, C.; Dressel, M.; Pronin, A.V. Two-channel conduction in YbPtBi. *Phys. Rev. B* **2017**, *95*, 155201. [[CrossRef](#)]
- Chaudhuri, D.; Cheng, B.; Yaresko, A.; Gibson, Q.D.; Cava, R.J.; Armitage, N.P. Optical investigation of the strong spin-orbit-coupled magnetic semimetal YbMnBi₂. *Phys. Rev. B* **2017**, *96*, 075151. [[CrossRef](#)]
- Neubauer, D.; Yaresko, A.; Li, W.; Löhle, A.; Hübner, R.; Schilling, M.B.; Shekhar, C.; Felser, C.; Dressel, M.; Pronin, A.V. Optical conductivity of the Weyl semimetal NbP. *Phys. Rev. B* **2018**, *98*, 195203. [[CrossRef](#)]
- Kemmler, R.; Hübner, R.; Löhle, A.; Neubauer, D.; Voloshenko, I.; Schoop, L.M.; Dressel, M.; Pronin, A.V. Free-carrier dynamics in Au₂Pb probed by optical conductivity measurements. *J. Phys.: Condens. Matter* **2018**, *30*, 485403. [[CrossRef](#)] [[PubMed](#)]
- Maulana, L.Z.; Manna, K.; Uykur, E.; Felser, C.; Dressel, M.; Pronin, A.V. Optical conductivity of multifold fermions: The case of RhSi. *Phys. Rev. Research* **2020**, *2*, 023018. [[CrossRef](#)]
- Maulana, L.Z.; Li, Z.; Uykur, E.; Manna, K.; Polatkan, S.; Felser, C.; Dressel, M.; Pronin, A.V. Broadband optical conductivity of the chiral multifold semimetal PdGa. *Phys. Rev. B* **2021**, *103*, 115206. [[CrossRef](#)]
- Dressel, M.; Gürner, G. *Electrodynamics of Solids*; Cambridge University Press: Cambridge, UK, 2002.
- Sachdev, S. *Quantum Phase Transitions*; Cambridge University Press: Cambridge, UK, 2011.
- Van der Marel, D.; Molegraaf, H.J.A.; Zaanen, J.; Nussinov, Z.; Carbone, F.; Damascelli, A.; Eisaki, H.; Greven, M.; Kes, P.H.; Li, M. Quantum critical behaviour in a high- T_c superconductor. *Nature* **2003**, *425*, 271–274. [[CrossRef](#)] [[PubMed](#)]
- Ioffe, L.B.; Millis, A.J. Zone-diagonal-dominated transport in high- T_c cuprates. *Phys. Rev. B* **1998**, *58*, 11631–11637. [[CrossRef](#)]
- Van der Marel, D. Anisotropy of the optical conductivity of high- T_c cuprates. *Phys. Rev. B* **1999**, *60*, R765. [[CrossRef](#)]

29. Anderson, P.W. Infrared conductivity of cuprate metals: Detailed fit using Luttinger-liquid theory. *Phys. Rev. B* **1997**, *55*, 11785–11788. [[CrossRef](#)]
30. Schilling, M.B.; Schoop, L.M.; Lotsch, B.V.; Dressel, M.; Pronin, A.V. Flat Optical Conductivity in ZrSiS due to Two-Dimensional Dirac Bands. *Phys. Rev. Lett.* **2017**, *119*, 187401. [[CrossRef](#)]
31. Brechtel, E.; Cordier, G.; Schäfer, H. Zur Darstellung und Struktur von CaMnBi_2 . *Z. Naturforsch. B* **1980**, *35*, 1–3. [[CrossRef](#)]
32. Sayetat, F.; Fertey, P.; Kessler, M. An Easy Method for the Determination of Debye Temperature from Thermal Expansion Analyses. *J. Appl. Cryst.* **1998**, *31*, 121–127. [[CrossRef](#)]